Three-dimensional inversion of transient EM data with IP effect

Xinchong Zhang, Changchun Yin
College of Geo-Exploration Science and Technology, Jilin University, zhangxc20@mails.jlu.edu.cn

SUMMARY

The transient electromagnetic (TEM) method, as a low-cost and high-efficiency exploration technology, plays an important role in the exploration of mineral resources. The polarizable bodies are often developed in metal deposits, and the induced polarization (IP) effect caused by them can distort the late-time signal in TEM data or even reverse its sign. The traditional inversion only considering resistivity can not effectively invert the data contaminated by the IP effect, which brings difficulties to the application of TEM in areas with IP. To solve this problem, we propose a three-dimensional (3D) TEM inversion method that takes into account the IP effect. The advantage of this method is that it can directly do forward and inverse modeling in the time domain without needing any transformation. Numerical experiments show that high-accuracy modeling results can be achieved, while the resistivity and chargeability of the model assumed can be inverted successfully. This proves the effectiveness of the method for the inversion of TEM data with the IP effect.

Keywords: Transient electromagnetic (TEM) method, three-dimensional (3D), inversion, induced polarization (IP) effect.

INTRODUCTION

The transient electromagnetic (TEM) method, as an important EM geophysical method, has been widely used in mineral exploration for its low cost and high efficiency. The polarizable bodies are commonly developed in metal deposits, such as massive sulfide ore bodies, copper-nickel ore bodies, graphite ore bodies, etc. Due to the existence of these polarizable bodies, the IP effect will distort the transient electromagnetic data at a late time and even reverse the sign. The traditional inversions only considering the resistivity cannot effectively invert these data containing the IP effect, which has caused obstacles to the application of TEM in these areas. Therefore, the study of TEM modeling and inversions considering the IP effect has extreme importance.

At present, the study on TEM one-dimensional (1D) inversion considering the IP effect has been relatively mature. Although the 1D method can quickly invert IP parameters, there are few layered structures assumed in 1D inversions existing in actual geological situations. When there are irregular 3D polarizable bodies or terrains, 1D inversions often provide wrong results, so it is very necessary to do 3D TEM inversion while considering the IP effect. At present, the frequency-time conversion method is used in most 3D TEM modeling and inversions. Whether it is in the forward modeling or the calculation of the Jacobian matrix, the frequency-domain responses are calculated in a frequency range and then converted to the time domain (Man et al., 2023). It is worth noting that the TEM data will have certain errors after the frequency-time transformations. In this paper, we present a direct time-domain inversion method. The forward solution and calculation of the Jacobian matrix are carried out directly in the time domain as well. Numerical experiments with synthetic data show that reliable resistivity and chargeability can be reliably obtained.

METHODS

Forward Modeling

From Maxwell's equations, the diffusion equation of the electric field can be written as

$$\nabla\times\nabla\times\boldsymbol{E}(\boldsymbol{r},t)+\mu\frac{\partial\,\boldsymbol{j}(\boldsymbol{r},t)}{\partial t}+\mu\frac{\partial\,\boldsymbol{j}_s(\boldsymbol{r},t)}{\partial t}=0 \quad .（1）$$

In a polarizable medium, the conductivity is variable, which leads to a more complicated description of Ohm's law. Especially when the IP effect occurs, the conductivity will change with frequency. To describe this phenomenon more accurately, Pelton et al. (1978) introduced the Cole-Cole model. The Cole-Cole model is a mathematical expression used to explain complex polarization effects in medium, which can better reveal the relationship between conductivity and frequency that can be written as

$$\sigma(\omega)=\sigma_0\left(1-m\left(1-\frac{1}{1+(i\omega\tau)^c}\right)\right)^{-1}, \quad (2)$$

where σ_0 is the DC conductivity, m is the chargeability, characterizing the intensity of the IP effect of the polarizable body, i is the imaginary unit, ω is the angular frequency, τ is the time constant, characterizing the charging and discharging speed of the polarizable body, c is the frequency-dependent coefficient, which represents the uniformity of minerals distributed in the polarizable body with the value range $0<c\leqslant 1$. Substitute Eq. (2) into Ohm's law, we obtain the expression of Ohm's law for a polarizable medium in the time domain, i.e.

$$\sigma_0\boldsymbol{E}(\boldsymbol{r},t)+\tau^c\sigma_0\frac{\partial^c\boldsymbol{E}(\boldsymbol{r},t)}{\partial t^c}=\boldsymbol{j}(\boldsymbol{r},t)+\tau^c(1-m)\frac{\partial^c\boldsymbol{j}(\boldsymbol{r},t)}{\partial t^c}. \quad (3)$$

The fractional derivatives appear at both ends of Eq. (3). We use the Caputo operator to discretize the fractional derivatives in the above equation (Zhang et al., 2022), which can be written as

$$\begin{aligned}&\sigma_0\boldsymbol{E}(\boldsymbol{r},t_k)+\tau^c\sigma_0\frac{1}{\Gamma(2-c)}\left\{\sum_{p=0}^{k-1}\frac{\boldsymbol{E}(\boldsymbol{r},t_{p+1})-\boldsymbol{E}(\boldsymbol{r},t_p)}{\Delta t_p}\left[(t_k-t_p)^{1-c}-(t_k-t_{p+1})^{1-c}\right]\right\}\\&=\boldsymbol{j}(\boldsymbol{r},t_k)+\tau^c(1-m)\frac{1}{\Gamma(2-c)}\left\{\sum_{p=0}^{k-1}\frac{\boldsymbol{j}(\boldsymbol{r},t_{p+1})-\boldsymbol{j}(\boldsymbol{r},t_p)}{\Delta t_p}\left[(t_k-t_p)^{1-c}-(t_k-t_{p+1})^{1-c}\right]\right\}\end{aligned}. \quad (4)$$

Furthermore, by substituting Eq. (4) into (1), and applying the vector finite-element method based on tetrahedral grids and the backward Euler scheme to discretize the space and time domain respectively, we obtain the forward equations as

$$\begin{bmatrix}\mathbf{D}_1 &&&&&&&\\ -\mathbf{C}_2^1 & \mathbf{D}_2 &&&&&&\\ -\mathbf{C}_3^2 & -\mathbf{C}_3^1 & \mathbf{D}_3 &&&&&\\ -\mathbf{C}_4^3 & -\mathbf{C}_4^2 & -\mathbf{C}_4^1 & \mathbf{D}_4 &&&&\\ \vdots & \vdots & \cdots & \vdots & \ddots &&&\\ -\mathbf{C}_{n-2}^{n-3} & -\mathbf{C}_{n-2}^{n-4} & \cdots & -\mathbf{C}_{n-2}^{2} & -\mathbf{C}_{n-2}^{1} & \mathbf{D}_{n-2} &&\\ -\mathbf{C}_{n-1}^{n-2} & -\mathbf{C}_{n-1}^{n-3} & \cdots & -\mathbf{C}_{n-1}^{3} & -\mathbf{C}_{n-1}^{2} & -\mathbf{C}_{n-1}^{1} & \mathbf{D}_{n-1} &\\ -\mathbf{C}_{n}^{n-1} & -\mathbf{C}_{n}^{n-2} & \cdots & -\mathbf{C}_{n}^{4} & -\mathbf{C}_{n}^{3} & -\mathbf{C}_{n}^{2} & -\mathbf{C}_{n}^{1} & \mathbf{D}_n\end{bmatrix}\begin{bmatrix}\boldsymbol{E}_1\\ \boldsymbol{E}_2\\ \boldsymbol{E}_3\\ \boldsymbol{E}_4\\ \vdots\\ \boldsymbol{E}_{n-2}\\ \boldsymbol{E}_{n-1}\\ \boldsymbol{E}_n\end{bmatrix}=\begin{bmatrix}\mathbf{b}_1\\ \mathbf{b}_2\\ \mathbf{b}_3\\ \mathbf{b}_4\\ \vdots\\ \mathbf{b}_{n-2}\\ \mathbf{b}_{n-1}\\ \mathbf{b}_n\end{bmatrix}. \quad (5)$$

Eq. (5) can be abbreviated as

$$\mathbf{K}\boldsymbol{E}=\boldsymbol{b}, \quad (6)$$

where **K** is the coefficient matrix, ***E*** is the electric fields to be solved at the edges of tetrahedral mesh elements and ***b*** is the source term. The TEM responses with the IP effect can be obtained by solving equation (6).

Inversions

Based on the theory of regularized inversion, the following objective function for 3D TEM inversions is constructed:

$$\varphi=\left\|\mathbf{C_d}\left(\mathbf{d}_{\text{obs}}-\mathbf{d}_{\text{pre}}\right)\right\|_2^2+\lambda\left\|\mathbf{C_m}\left(\mathbf{m}-\mathbf{m}_0\right)\right\|_2^2, \quad (7)$$

where $\mathbf{d}_{\text{obs}}$ is the observation data, and $\mathbf{d}_{\text{pre}}$ is the forward response. $\mathbf{C}_{\text{d}}$ is the data covariance matrix, which is a diagonal matrix related to the data error. **m** is the model parameters, and $\mathbf{m}_0$ is the reference model. $\mathbf{C}_{\text{m}}$ is the model roughness operator.

By calculating the first order of the partial derivative concerning the model parameter **m** at both ends of the objective function, we obtain the gradient of the objective function, i.e.

$$\mathbf{g}=-2\mathbf{J}^{\mathrm{T}}\mathbf{C}_{\mathbf{d}}^{\mathrm{T}}\mathbf{C}_{\mathbf{d}}\left(\mathbf{d}_{\text{obs}}-\mathbf{d}_{\text{pre}}\right)+2\lambda\mathbf{C}_{\mathbf{m}}^{\mathrm{T}}\mathbf{C}_{\mathbf{m}}(\mathbf{m}-\mathbf{m}_0). \quad (8)$$

The transpose of the Jacobian matrix $\mathbf{J}^{\mathrm{T}}$ in Eq. (8) can be expressed as

$$\mathbf{J}^{\mathrm{T}}=-\left(\frac{\partial\mathbf{K}_t}{\partial\mathbf{m}}\boldsymbol{E}-\frac{\partial\mathbf{s}_t}{\partial\mathbf{m}}\right)^{\mathrm{T}}\left(\mathbf{K}_t{}^{\mathrm{T}}\right)^{-1}\mathbf{L}^{\mathrm{T}}. \quad (9)$$

From the definition of the interpolation operator L, we can see that direct calculation and storing of the transpose of the Jacobian matrix consumes a lot of time and memory. To avoid this problem, we use the adjoint forward modeling method in the time domain to obtain the transpose of the Jacobian matrix implicitly, i.e.

$$\mathbf{J}^{\mathrm{T}}\mathbf{r}_d=-\left(\frac{\partial\mathbf{K}_t}{\partial\mathbf{m}}\boldsymbol{E}-\frac{\partial\mathbf{s}_t}{\partial\mathbf{m}}\right)^{\mathrm{T}}\left(\mathbf{K}_t{}^{\mathrm{T}}\right)^{-1}\mathbf{L}^{\mathrm{T}}\mathbf{r}_d. \quad (10)$$

Introducing a new parameter $\mathbf{u}_d$, namely

$$\mathbf{u}_d=(\mathbf{K}_t{}^{\mathrm{T}})^{-1}\mathbf{L}^{\mathrm{T}}\mathbf{r}_d, \quad (11)$$

then, after a simple calculation, we can get

$$\mathbf{K}_t{}^{\mathrm{T}}\mathbf{u}_d=\mathbf{L}^{\mathrm{T}}\mathbf{r}_d. \quad (12)$$

The expansion of Eq. (12) can be expressed as

$$\begin{bmatrix}\mathbf{D}_1 & -\mathbf{C}_2^1 & -\mathbf{C}_3^2 & -\mathbf{C}_4^3 & \cdots & -\mathbf{C}_{n-2}^{n-3} & -\mathbf{C}_{n-1}^{n-2} & -\mathbf{C}_n^{n-1}\\ & \mathbf{D}_2 & -\mathbf{C}_3^1 & -\mathbf{C}_4^2 & \cdots & -\mathbf{C}_{n-2}^{n-4} & -\mathbf{C}_{n-1}^{n-3} & -\mathbf{C}_n^{n-2}\\ && \mathbf{D}_3 & -\mathbf{C}_4^1 & \cdots & \vdots & \vdots & \vdots\\ &&& \mathbf{D}_4 & \cdots & -\mathbf{C}_{n-2}^2 & -\mathbf{C}_{n-1}^3 & -\mathbf{C}_n^4\\ &&&& \ddots & -\mathbf{C}_{n-2}^1 & -\mathbf{C}_{n-1}^2 & -\mathbf{C}_n^3\\ &&&&& \mathbf{D}_{n-2} & -\mathbf{C}_{n-1}^1 & -\mathbf{C}_n^2\\ &&&&&& \mathbf{D}_{n-1} & -\mathbf{C}_n^1\\ &&&&&&& \mathbf{D}_n\end{bmatrix}\begin{bmatrix}\boldsymbol{u}_1\\ \boldsymbol{u}_2\\ \boldsymbol{u}_3\\ \boldsymbol{u}_4\\ \vdots\\ \boldsymbol{u}_{n-2}\\ \boldsymbol{u}_{n-1}\\ \boldsymbol{u}_n\end{bmatrix}=\begin{bmatrix}\mathbf{r}_1\\ \mathbf{r}_2\\ \mathbf{r}_3\\ \mathbf{r}_4\\ \vdots\\ \mathbf{r}_{n-2}\\ \mathbf{r}_{n-1}\\ \mathbf{r}_n\end{bmatrix}. \quad (13)$$

After calculating the sensitivity information, the gradient of the objective function can be obtained. We apply the limited-memory quasi-newton method (Liu et al. 1989) to optimize Eq. (7) until the data fitting errors reduce to a certain level, and then we can obtain the final inversion model.

RESULTS

Model design

To verify the effectiveness of our method, we design a horizontal slab with a size of 100×100×30 m and a central depth of 60 m for our numerical experiments. Referring to Figure 1, we set up a 200*200 m transmission loop at the earth's surface and 9 survey lines with a station and line distance of 20 m. A total of 81 measuring points are created. We use unstructured tetrahedrons to discretize the model domain and create 386610 elements for the forward modeling as shown in Figure 2(a), and 322,643 elements for inversions as shown in Figure 2(b).

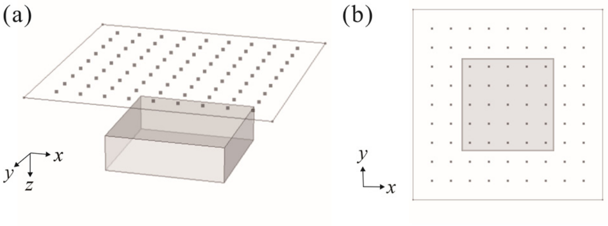

Figure 1. Layout of TEM system.

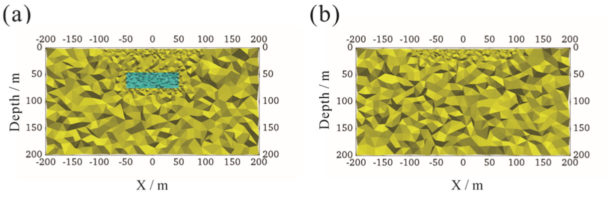

Figure 2. Generation of unstructured tetrahedral mesh for (a) forward modeling, and (b) Inversions.

Resistivity inversion

Firstly, we invert the resistivity of the above model in 3D. The resistivity of the slab is 1 ohm-m, the resistivity of the surrounding rock is 100 ohm-m, and other IP parameters of the surrounding rock and slab remain the same, with a chargeability of 0.1, a time constant of 0.01 s, and a frequency-dependent coefficient of 0.6. By adding 3% Gaussian noise to dB_z/dt data calculated by a 3D forward modeling method, the 3D inversion is carried out to the model data contaminated with noise. Figure 3 shows the inversion results along profile Y=0 m and a depth of 60 m, respectively, where the black box marks the outline of the true model. It can be seen from the figure that the inversion results show the position and size of the horizontal slab well, and the boundary is clearly observed. At the same time, the resistivity of the horizontal slab obtained by inversion is very close to the true value.

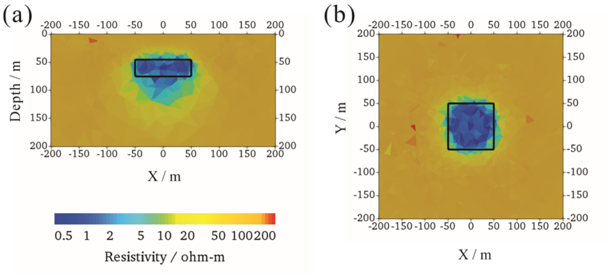

Figure 3. The inverted resistivity of a horizontal slab model. (a) Profile at Y=0 m; (b) profile at the depth of 60 m.

Chargeability inversion

We further carried out 3D inversions for the chargeability of the above-designed model. It is assumed that the chargeability of the slab is 0.5, the chargeability of the surrounding rock is 0.1, and other IP parameters of the surrounding rock and the slab remain the same as in Figure 2, with a resistivity of 100 ohm-m, a time constant of 0.01 s, and a frequency-dependent coefficient of 0.6. By adding 1% Gaussian noise to dB_z/dt data obtained by the 3D forward modeling method, the 3D inversion is carried out to the noise-contaminated data. Figure 4 shows the inversion results in profile at Y=0 m or at a depth of 60 m, respectively, where the black box marks the outline of the true model. It is seen from the figure that the inversion results describe the position and size of the horizontal slab well, and the boundary can be roughly delineated. Meanwhile, the chargeability of the horizontal slab obtained by the inversion is very close to the true value.

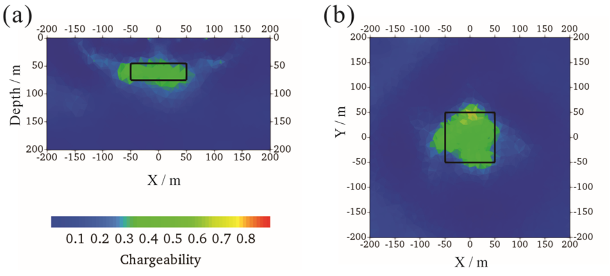

Figure 4. The inverted chargeability for the horizontal slab model. (a) Profile at Y=0 m; (b) profile at the depth of 60 m.

Simultaneous inversion of resistivity and chargeability

Finally, a simultaneous 3D inversion of the resistivity and chargeability of the above-designed model is carried out. The resistivity of the slab is 1 ohm-m and the chargeability is 0.5, the resistivity of the surrounding rock is 100 ohm-m and the chargeability is 0.1. The other IP parameters of the surrounding rock and the slab remain the same as in Figure 2, with a time constant of 0.01 s, and a frequency-dependent correlation coefficient of 0.6. By adding 5% Gaussian noise to dB_z/dt data calculated using a 3D forward modeling method, the 3D inversion is carried out to the noise-contaminated data. Figure 5 shows the inversion results of resistivity and chargeability in profile Y=0 m and at the depth of 60 m. The black boxes mark the outline of the real model. It can be seen from Figures 5(a) and 5(b) that the inversion results can roughly describe the position and distribution of the horizontal slab and delineate the horizontal boundary to some extent, while the resistivity of the horizontal slab obtained by the inversion is close to the true value. From Figures 5(c) and 5(d), it is seen that the inversion results can roughly describe the position and size of the horizontal slab, and the horizontal boundary can be roughly delineated. The chargeability of the horizontal slab obtained by the inversion is close to the real value. The numerical example verifies the effectiveness of the inversion method for the detection of low-resistivity and high-chargeability slabs.

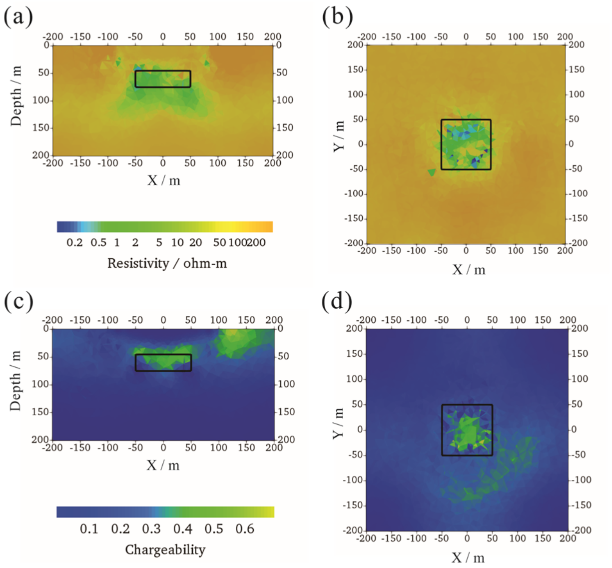

Figure 5. The inverted resistivity and polarizability for the horizontal slab model. (a) Resistivity profile at Y=0 m; (b) resistivity profile at the depth of 60 m; (c) chargeability profile at Y=0 m; (d) chargeability profile at the depth of 60 m.

CONCLUSIONS

In this paper, we have successfully developed a 3D inversion method for TEM data with the IP effect by introducing the Caputo operator to discretize the fractional derivatives in the time domain. The effectiveness of the proposed method is verified by numerical experiments on a model of a horizontal slab. The proposed method can invert the position and size of the anomalous body, and the resistivity and chargeability of the target body can also be well inverted. We will also conduct inversion studies on other IP parameters as well as complex models, which will be presented at the workshop.

ACKNOWLEDGEMENTS

The study is financially supported by the National Natural Science Foundation of China (42030806).

REFERENCES

Liu DC, Nocedal J (1989) On the limited memory BFGS method for large scale optimization. Math Program 45: 503-528.

Man K F, Yin C C, Liu Y H, Sun S Y, Xiong B (2023) 3D inversion of time-domain airborne EM data for IP parameters. Chinese J. Geophys. (in Chinese) 66(3): 1269-1280.

Pelton W H, Ward S H, Hallof P G, Sill W R, Nelson P H (1978). Mineral discrimination and removal of inductive coupling with multifrequency IP. Geophysics, 43(3): 588.

Xinchong Zhang, Changchun Yin, Luyuan Wang, Yang Su, Yunhe Liu (2022) 3D Time-Domain Airborne EM Forward Modeling with IP effect Based on Implicit Difference Discretization of Caputo Operator. IEEE Transactions on Geoscience and Remote Sensing 60: 1.